Full Paper

CONTRAST MEDIA & MOLECULAR IMAGING

Received: 24 February 2012, Revised: 31 October 2012, Accepted: 11 December 2012, Published online in Wiley Online Library

(wileyonlinelibrary.com) DOI: 10.1002/cmmi.1528

Regional heterogeneity changes in DCE-MRI as response to isolated limb perfusion in experimental soft-tissue sarcomas

L. Alic[a,b]*, M. van Vliet[a], P. A. Wielopolski[a], T. L. M. ten Hagen[c], C. F. van Dijke[a], W. J. Niessen[a,b,d] and J. F. Veenland[a,b]

ABSTRACT: Experimental evidence supports an association between heterogeneity in tumor perfusion and response to chemotherapy/radiotherapy, disease progression and malignancy. Therefore, changes in tumor perfusion may be used to assess early effects of tumor treatment. However, evaluating changes in tumor perfusion during treatment is complicated by extensive changes in tumor type, size, shape and appearance. Therefore, this study assesses the regional heterogeneity of tumors by dynamic contrast-enhanced MRI (DCE-MRI) and evaluates changes in response to isolated limb perfusion (ILP) with tumor necrosis factor alpha and melphalan. Data were acquired in an experimental cancer model, using a macromolecular contrast medium, albumin–(Gd–DTPA)45. Small fragments of BN 175 (a soft-tissue sarcoma) were implanted in eight brown Norway rats. MRI of five drug-treated and three sham-treated rats was performed at baseline and 1 h after ILP intervention. Properly co-registered baseline and follow-up DCE-MRI were used to estimate the volume transfer constant (K^{trans}) pharmacokinetic maps. The regional heterogeneity was estimated in 16 tumor sectors and presented in cumulative map-volume histograms. On average, ILP-treated tumors showed a decrease in regional heterogeneity on the histograms. This study shows that heterogenic changes in regional tumor perfusion, estimated using DCE-MRI pharmacokinetic maps, can be measured and used to assess the short-term effects of a potentially curative treatment on the tumor microvasculature in an experimental soft-tissue sarcoma model. Copyright © 2013 John Wiley & Sons, Ltd.

Keywords: dynamic contrast-enhanced magnetic resonance imaging; isolated limb perfusion; tumor heterogeneity; soft-tissue sarcoma treatment

1. INTRODUCTION

Increased use of current anti-angiogenic agents and development of novel ones for cancer treatment pose new challenges to medical imaging technologies. In contrast to the systemic effect of traditional cytotoxic drugs, these new agents selectively target the endothelial cells of tumor neovasculature (1–3). Although often costly, these treatments are potentially effective and have become a priority for oncologists and pharmaceutical companies.

Low local concentration of anti-tumor agents and dose-limiting toxicity are often the cause of failure of chemotherapy. In isolated limb perfusion (ILP), local drug concentrations are increased while systemic exposure to the drug is minimal (4). By utilizing ILP, tumors are exposed to concentrations up to 15–20 times higher than the maximum tolerated dose of tumor necrosis factor alpha (TNF-α) without major side-effects. TNF-α also has an indirect effect on endothelial cells and tumor-associated vasculature (5–7). By combining TNF-α with a cytostatic drug (e.g. melphalan), an immediate TNF-mediated tumor-selective enhanced drug uptake can be realized (8,9). This effect depends on the vascularization of the tumor and is followed by a tumor-selective permeabilization and eradication of the tumor-associated vasculature (10,11).

Dynamic contrast-enhanced magnetic resonance imaging (DCE-MRI) enables the noninvasive characterization of tumors, and has emerged as a valuable tool for monitoring pathophysiologic changes in various aspects of tumor vascular structure and function (12,13). DCE-MRI with macromolecular contrast media (MMCM) depicts microvessel permeability (14) and has been shown in experimental models to express tumor perfusion solely owing to malfunctioning tumor vessels (5,15).

Experimental evidence shows the association of tumor vascular heterogeneity with disease progression and malignancy (3). Heterogeneity of tumor blood supply results in the formation of hypoxic voids associated with oxidative stress, promotion of

* *Correspondence to: L. Alic, Erasmus MC – University Medical Centre Rotterdam, Department of Medical Informatics, Rotterdam, The Netherlands. Email: LejlaResearch@gmail.com*

a *L. Alic, M. van Vliet, P. A. Wielopolski, C. F. Dijke, W. J. Niessen, J. F. Veenland*
Erasmus MC – University Medical Centre Rotterdam, Department of Medical Informatics, Rotterdam, The Netherlands

b *L. Alic, W. J. Niessen, J. F. Veenland*
Erasmus MC - University Medical Centre Rotterdam, Department of Radiology, Rotterdam, The Netherlands

c *T. L. M. Hagen*
Erasmus MC - University Medical Centre Rotterdam, Department of Experimental Surgical Oncology, Rotterdam, The Netherlands

d *W. J. Niessen*
Delft University of Technology, Imaging Science and Technology, Faculty of Applied Sciences, Delft, The Netherlands

survival factors and genomic instability (16). This indicates the importance of tumor vascular heterogeneity for disease mechanism and possibly will lead to the discovery of novel treatment strategies. A heterogeneous blood supply will also affect treatment response owing to poor delivery of chemotherapeutic agents to areas of low vascularity. The importance of neovascular heterogeneity for tumor treatment is well documented (3,17,18). Although the use of tumor heterogeneity as a biomarker for treatment response has been evaluated (19–21), these studies summarize tumor heterogeneity across the whole tumor and thereby fail to identify regional changes.

An alternative approach is to deal with intratumoral heterogeneity at the sub-tumor level. This method partitions a tumor into volumes of interest (VOI) based on certain tumor properties, such as identifying regions with bulky enhancement, that is, the 'hot-spot'. This has been performed either manually (22–24) or by thresholding a parameter value or a fit statistic (25,26). Another approach, inspired by the strong peripheral tumor enhancement common in solid tumors, involves tumor segmentation into concentric bands (5,27–30). However, the number and size of those bands is rather arbitrary, and these studies do not account for the heterogeneity within such a concentric band.

The present preclinical study evaluates the potential of heterogeneity, in DCE-MRI with MMCM, as a biomarker for the early effect of a combined cancer treatment with TNF-α and melphalan in an experimental model of soft-tissue sarcoma. The changes in temporal pattern of signal enhancement owing to MMCM are expected to reflect changes owing to treatment. Following change in the tumor over time requires properly co-registered baseline to follow-up pairs, which is complicated by extensive changes in tumor size, tumor shape and DCE-MRI appearance. This makes it difficult to analyze tumors on a complete voxel-wise level. Therefore, we assessed the regional changes in DCE-MRI parametric maps that were co-registered to facilitate such an analysis. To quantify tumor heterogeneity, we introduce the cumulative map-volume (CMV) histogram. Although hemorrhagic necrosis and destruction of the endothelial cells will develop in time after TNF-α administration, we hypothesize that the effect of ILP intervention will be evident 1 h after initiation.

2. RESULTS

When implanted subcutaneously in the hind limb, the fragments of the syngenic BN175 soft-tissue sarcoma grew into tumors that appeared as masses composed of several lobes. Figure 1 shows the features of a lobular carcinoma with viable tumor parts (A) and less viable tumor parts (B). Tumor growth rates mirrored those previously published (5,8), with an average post inoculation growth period of two weeks to reach 15 mm in diameter.

Co-registered baseline and follow-up DCE-MRI were used to estimate the pharmacokinetic maps of the volume transfer constant (K^{trans}). To estimate K^{trans} ($\mu l\ s^{-1}$) accurately, we assessed all components at baseline and follow-up separately. The voxel-wise tumor native longitudinal relaxation time ($T_{1,0}$) was estimated prior to the administration of contrast agent. The vascular input function (VIF) was estimated after the administration of contrast agent. To quantify the effect of tumor treatment, we evaluated the slope of the CMV histogram for the 16 tumor regions, only considering the enhancing fraction. DCE-MRI-derived maps from a tumor before (top row) and 1 h after the intervention (bottom row) are shown in Fig. 2 for ILP intervention with TNF-α and melphalan and in Fig. 3 for sham intervention. Panels A and D (for both figures) show a maximum intensity projection (MIP) of the late-stage enhanced image with arrows illustrating a VIF VOI position. Consecutive columns (in both Figs 2 and 3) represent the $T_{1,0}$ map before contrast agent administration (B and E), and the K^{trans} map (C and F).

2.1. Longitudinal Relaxation Rate $R_{1,0}$

For the VIF VOI, the average $T_{1,0} = 1/R_{1,0}$ at baseline was equal to 1.44 ± 0.13 s. The average $T_{1,0}$ after the ILP intervention was 1.98 ± 0.12 s for animals treated with TNF-α and melphalan, and 1.30 ± 0.06 s for animals treated with sham perfusion. For all fits, r^2-values were within the range of 0.61–0.99 (mean $r^2 = 0.88 \pm 0.14$). These results are similar to previous measurements in rat blood (5,31).

For the tumor VOI the average $T_{1,0} = 1/R_{1,0}$ at baseline was 1.16 ± 0.2 s. The $T_{1,0}$ after the ILP intervention was 0.72 ± 0.12 s for animals treated with TNF-α and melphalan, and 1.07 ± 0.15 s for animals after sham perfusion. Figure 2 shows the $T_{1,0}$ tumor map at baseline (B) and at follow-up (E) for an animal after ILP intervention with TNF-α and melphalan. Figure 3 shows the $T_{1,0}$ tumor map at baseline (B) and at follow-up (E) for an animal after sham intervention.

2.2. Pharmacokinetics

Regardless of the treatment category (i.e. treated or control), the intervention significantly decreases the enhancing fraction of the tumor from $78.02 \pm 11.46\%$ at baseline to $42.71 \pm 23.32\%$ at follow-up. There was no significant difference, in enhancing fraction, at baseline and at follow-up between the treatment categories or between the regions. Similar effects were observed

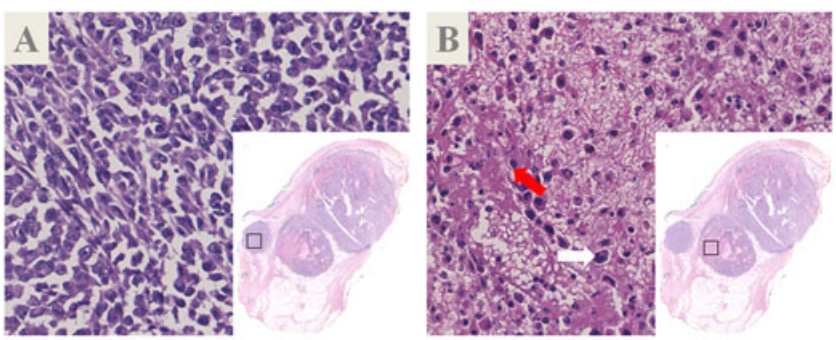

Figure 1. Morphology of syngenic BN175 soft-tissue sarcoma showing viable parts (A) and less viable parts (B) with good developed nuclei (white arrow) and pyknotic nuclei (red arrow).

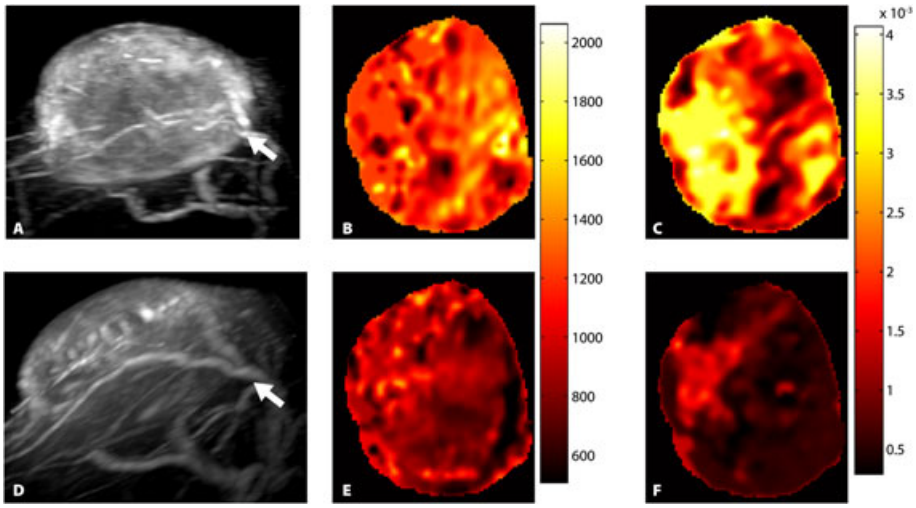

Figure 2. A tumor before (top row) and after (bottom row) isolated limb perfusion (ILP) intervention with tumor necrosis factor alpha (TNF-α) and melphalan. First column (A and D) shows a maximum intensity projection (MIP) of the late stage enhanced image with arrows illustrating position of a VIF VOI. Consecutive columns represent T_{10} map before contrast agent administration (B and E), and K^{trans} map (C and F).

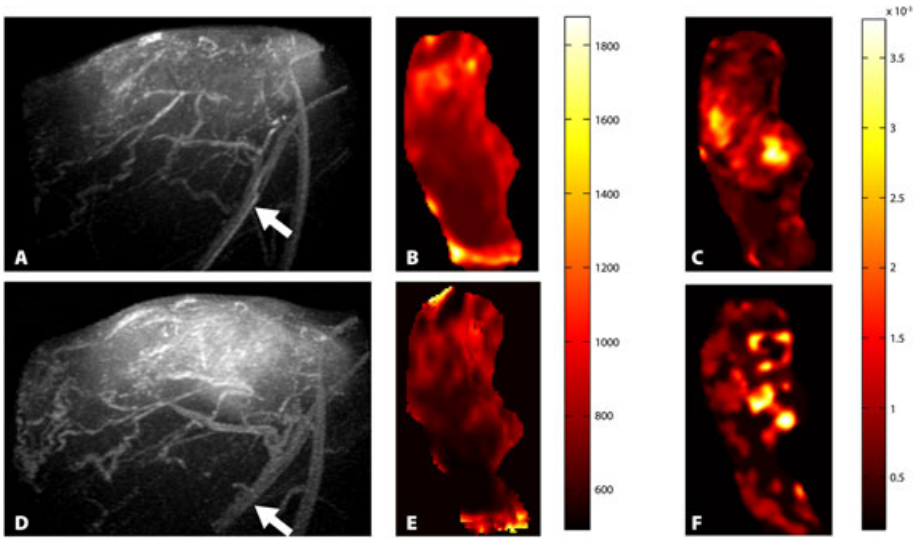

Figure 3. A tumor before (top row) and after (bottom row) sham intervention. First column (A and D) shows a maximum intensity projection (MIP) of the late stage enhanced image with arrows illustrating a position of vascular input function (VIF) voxel of interest (VOI). Consecutive columns represent T_{10} map before contrast agent administration (B and E), and K^{trans} map (C and F).

in the tumor core (79.24 ± 15.04 at baseline and 40.76 ± 26.87 at follow-up), the tumor periphery (77.43 ± 11.28 at baseline and 43.12 ± 22.63 at follow-up) and the tumor rim (73.53 ± 9.63 at baseline and 48.09 ± 18.66 at follow-up).

Table 1 presents the results for the mean estimated K^{trans} for different VOIs, before and after intervention. Figure 2 (ILP intervention with TNF-α and melphalan) and Fig. 3 (sham intervention) show the K^{trans} tumor map before (C) and after (E) the intervention. The Mann–Whitney *U*-test was used to assess significant differences in parametric maps between the response categories (treated and sham) as measured before and after the intervention separately. For all VOIs, the mean K^{trans} at baseline showed no significant difference between treatment and sham intervention. On the other hand, the mean K^{trans} at follow-up showed a significant difference between treatment and sham intervention ($p = 0.036$). In addition, the difference in parametric maps at baseline and follow-up was assessed using the Wilcoxon signed rank test for the treatment and sham groups. The mean K^{trans} at follow-up was significantly different from baseline for treatment intervention ($p = 0.04$), but not significantly different for sham intervention. For animals treated with TNF-α and melphalan, K^{trans} decreased in all VOIs. Figure 4 shows the box plots of K^{trans} at baseline and follow-up for both categories: that is, treated (TNF-α and melphalan) and sham.

Table 1. Mean K^{trans} before and after isolated limb perfusion intervention for both treatment categories (TNF-α and melphalan, and sham)

K^{trans} mean	Treated		Sham	
	Baseline	Follow-up	Baseline	Follow-up
Tumor whole	1.59 ± 0.43	$0.62 \pm 0.17^{*\S}$	1.84 ± 0.98	1.85 ± 0.94
Tumor rim	1.53 ± 0.37	$0.61 \pm 0.17^{*\S}$	1.66 ± 0.88	1.96 ± 0.90
Tumor core	1.56 ± 0.48	$0.62 \pm 0.17^{*\S}$	1.94 ± 0.87	1.69 ± 1.16
Tumor periphery	1.60 ± 0.41	$0.62 \pm 0.17^{*\S}$	1.80 ± 1.00	1.91 ± 0.89

*Significantly different from baseline value, and §significantly different from control group. Statistical significance was set at $p < 0.05$.

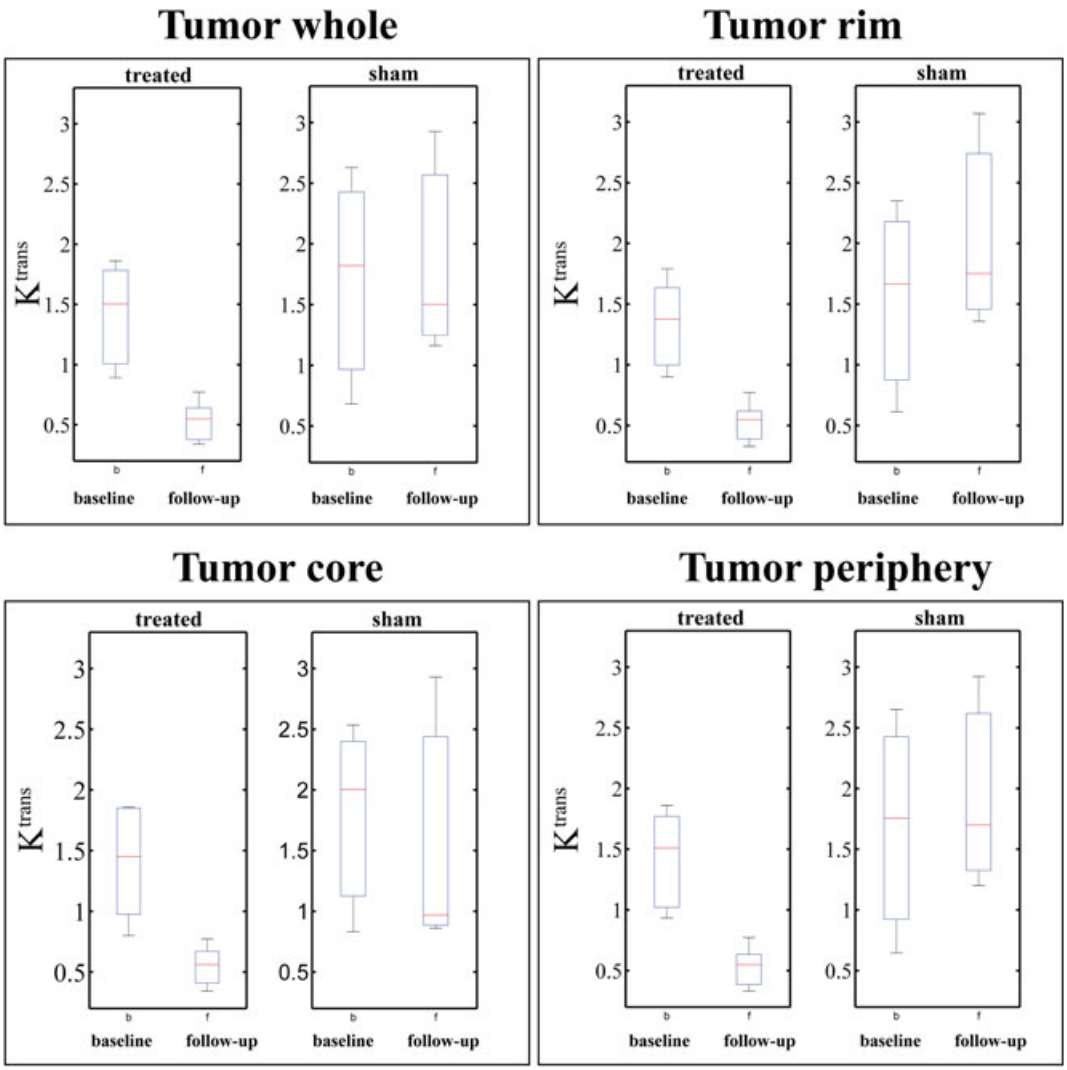

Figure 4. The box plots of K^{trans} at baseline and follow-up examinations for both categories; that is, treated (TNF-α and melphalan) and sham. Treated group showed statistically significant difference between baseline and follow-up (Wilcoxon signed rank test, $p < 0.05$) or all four VOIs; that is, tumor whole, tumor rim, tumor core and tumor periphery.

2.3. Sector Results

Figure 5 clearly shows the distinction between animals treated with TNF-α and melphalan, and animals treated with sham perfusion. This scatter plot shows the mean K^{trans} per sector, at baseline and at follow-up, for all tumors. The mean was computed for the voxels belonging to the enhancing fraction. For the TNF-α and melphalan-treated animals, a clear decrease in K^{trans} variance owing to treatment. For the sham-treated animals, the variance seems to increase. The average CMV histogram of the K^{trans} parametric map is plotted in Fig. 6 for TNF-α and melphalan-

treated animals (blue), and for sham-treated animals (red). Each of the 16 sectors was used to create 16 CMV histograms which were averaged afterwards. The dotted lines represent the standard deviation pooled over all sectors and all rats.

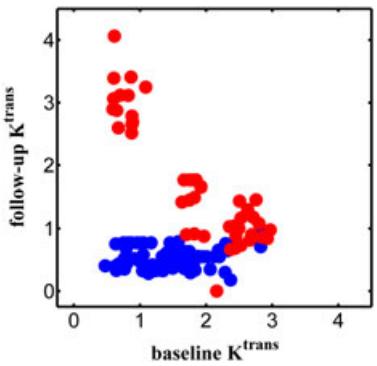

Figure 5. Scatter plot showing mean K^{trans} per sector (estimated for the voxels belonging to the enhancing fraction) at baseline and follow-up for both categories: TNF-α and melphalan-treated (blue) and sham-treated (red).

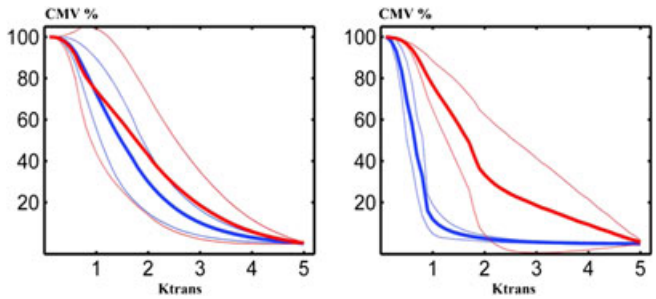

Figure 6. Cumulative map-volume (CMV) histogram representing the 3D-map distribution of K^{trans} for the whole tumor enhancing voxels as averaged over 16 predefined sectors. Blue line demonstrates averaged CMV histogram (solid line) and its deviation (dotted line) for all treated animals and all 16 sectors. Red line demonstrates the same information as blue line but for all sham animals. On the left are the results at baseline and on the right are the results at follow-up.

The CMV histogram values (Table 2) were fitted linearly as a function of K^{trans}, in a least squares sense, for three K^{trans} categories. The Mann–Whitney *U*-test was used to assess differences in the slope of the CMV histogram between the response categories (treated and sham) as measured before and after the intervention separately. At baseline, the slopes showed no significant difference between treatment and sham intervention. At follow-up, on the other hand, the slopes for all K^{trans} categories showed significant differences between treatment and sham intervention. For the follow-up examination, the difference in the slope of the CMV histogram at baseline and follow-up was assessed using the Wilcoxon signed rank test for the two separate groups, that is treatment and sham. For all K^{trans} categories, the slopes of the CMV histogram were significantly different from baseline for treatment intervention but not significantly different for sham intervention. The variance in the slopes over the regions is a measure for tumor heterogeneity. The standard deviation between the sectors, for the K^{trans} values ranging from 1–5 μl s^{-1}, decreases owing to treatment (Table 2). This is also illustrated in Fig. 6: the variance between the sectors for the drug-treated rats decreased after treatment whereas the variance of the sham-treated rats is similar to the variance before treatment. This implies the treatment induced homogenization of all tumor sectors with respect to K^{trans} values higher than 1 μl s^{-1}.

3. DISCUSSION AND CONCLUSIONS

Experimental evidence shows that, for several treatment alternatives, perfusion heterogeneity is associated with cancer treatment outcome (3,29). The present preclinical study evaluates the short-term effects of ILP intervention, that is, 1 h after the intervention. This allows assessment of the almost immediate effects of ILP on the microvasculature. Data from this pilot study indicate that the effects of ILP treatment can be successfully monitored by DCE-MRI 1 h after the intervention: in the treatment group the volume transfer constant (K^{trans}) decreased significantly after treatment with TNF-α and melphalan, whereas in the sham group no decrease in K^{trans} was observed.

To assess tumor heterogeneity we separated the tumor in several different VOIs; that is, tumor rim, tumor core, tumor periphery. Tumor core and periphery were each subdivided, using three orthogonal planes, into eight sectors. The 16 sectors, as such,

Table 2. The first order statistics for the slope of the cumulative map-volume (CMV) histogram over the 16 different sectors, before and after isolated limb perfusion intervention for both categories (TNF-α and melphalan-treated, and sham-treated)

CMV histogram slope	Treated		Sham	
	Baseline	Follow-up	Baseline	Follow-up
Mean (sectors)				
$(0 < K^{trans} < 1)$	-33.70 ± 25.45	$-109.57 \pm 9.37^{*\S}$	-30.75 ± 45.33	-33.29 ± 26.23
$(1 < K^{trans} < 2)$	-39.76 ± 8.20	$-6.14 \pm 5.37^{*\S}$	-30.86 ± 13.92	-37.76 ± 21.02
$(2 < K^{trans} < 5)$	-8.52 ± 5.79	$-0.66 \pm 0.64^{*\S}$	-13.49 ± 11.74	-9.99 ± 12.87
Standard deviation (sectors)				
$(0 < K^{trans} < 1)$	16.13 ± 10.28	13.55 ± 6.92	7.98 ± 8.80	16.78 ± 10.43
$(1 < K^{trans} < 2)$	12.04 ± 4.65	$4.83 \pm 3.69^{*\S}$	9.64 ± 4.59	15.74 ± 5.83
$(2 < K^{trans} < 5)$	4.26 ± 3.40	$0.66 \pm 0.56^{*}$	4.09 ± 3.40	2.61 ± 2.28

*Significantly different from baseline value, and §significantly different from control group. Statistical significance was set at $p < 0.05$.

have no pathophysiological meaning; they are a tool to study the heterogeneity in the tumor. The tumor rim was used since the rim is, generally, the most vascularized region of a solid tumor (5).

The tumor VOIs are selected after careful co-registration of pharmacokinetic maps, before and after the intervention. Therefore, we were able to pinpoint the region-based tumor treatment changes. To neatly summarize the gray value distribution of the estimated pharmacokinetic map, we exploited the CMV histogram by estimating its slope for three different K^{trans} categories, and for all 16 regions. The variance in the slopes over the regions is a measure for tumor heterogeneity. Our results show that the heterogeneity between the sectors for the K^{trans} values, ranging from 1 to 5 $\mu l\ s^{-1}$, decreases owing to treatment. This implies that the treatment induces tumor homogenization with respect to K^{trans} values higher than 1 $\mu l\ s^{-1}$. This regional analysis could be a helpful tool in evaluating local treatment effect. When part of the tumor 'escapes' from treatment, this can be detrimental for the whole treatment effect. With a regional analysis this 'escape' could be spotted within hours after start of treatment.

The ILP intervention is generally applied for the treatment of limb-threatening sarcomas and melanomas. During treatment, the limb is isolated from the systemic circulation. After perfusion the physiological limb perfusion is restored. The results show that, owing to the intervention, in both the drug-treated and the sham group, the enhancing fraction is decreased. The strength of this intervention is a combined effect of tumor necrosis factor alpha (TNF-α) and an alkylating agent (melphalan) intended to kill tumor cells. TNF-α augments the drug levels, within the tumor, via an increase of the melphalan concentration by six times (8,32,33). This strong effect increases the tumor cell eradication. TNF-α increases the vascular permeability of the tumor vessels already early during the perfusion while the quiescent vasculature of the healthy tissue is not affected. TNF-α may also induce hemodynamic changes. Both agents induce a cascade of effects in the tumor microenvironment. However, which combination of biological effects cause the decrease in K^{trans} is not clear. For instance, vessel disintegration or increased interstitial pressure could play a role.

For an accurate K^{trans} computation, a reliable $T_{1,0}$ estimation is a prerequisite. *In vivo* estimation of blood $T_{1,0}$, and thereby also VIF, is a nontrivial problem as it is susceptible for motion, system imperfections, in-flow effects and partial volume effects. To estimate K^{trans} as accurately as possible, we accounted for these problems as follows. The inoculation location, the hind limb, was chosen in order to minimize tumor movement during scanning. To estimate $T_{1,0}$, we selected a flow compensated inversion recovery gradient echo planar imaging sequence (IR-GE EPI). The IR technique is relatively immune for the system imperfections such as radio frequency (RF) power and slice imperfections (34). With GE EPI, a shorter acquisition time was possible compared with standard IR scans (GE or SE). We have selected a VOI far from a big artery with the consequence that the remaining blood flow in this VOI is slow enough to prohibit signal dephasing. The geometric distortions, owing to GE-EPI readout, were corrected for in the carefully performed co-registration procedure.

Even though a limited number of animals was examined, the data from this study support the hypothesis that the tumor heterogeneity patterns in the volume transfer constant as measured with CMV are an appropriate measure of tumor changes in response to ILP intervention. Therefore, the CMVs at can serve as noninvasive early outcome predictors in treatment monitoring and may guide therapy adaptation.

In summary, the present preclinical study suggests that heterogeneity in DCE-MRI pharmacokinetic maps can be used as a potential biomarker to quantify short-term effects of ILP intervention on tumor microvasculature in an experimental model of soft-tissue sarcoma. This provides reliable assessment of tumor treatment effect within 1 h after the ILP intervention. Further assessment of treatment effects requires comparative studies of ILP over different time points using registered DCE-MRI pharmacokinetic maps to histological sections.

4. MATERIAL AND METHODS

4.1. Animal and Tumor Model

Eight male inbred BN strain rats (Harlan-CPB, Austerlitz, the Netherlands), with a mean body weight of 300 g were implanted subcutaneously, in the hind limb, with 4 mm fragments of the syngenic BN175 soft-tissue sarcoma. The animals were inspected daily for tumor growth and general appearance. The tumors were imaged by MRI when they reached approximately 15 mm in diameter. Prior to MRI, the animals were randomly assigned to the drug-treated group (five) or sham-treated group (three). They were anesthetized with subcutaneous injection of 150 μl of a 1: 1 (v: v) mixture of ketamine (Alfasan, Woerden, The Netherlands) and xylazine (Bayer AG, Leverkusen, Germany). A 25-gage butterfly cannula was inserted into a tail vein for injection of contrast medium. The study was conducted with the approval of the local Committee for Animal Research.

4.2. Magnetic Resonance Contrast Media

Albumin–$(Gd–DTPA)_{45}$ is a water-soluble MMCM with a molecular weight of 92 kDa which corresponds to about 45 molecules of Gd–DTPA covalently bound to each albumin molecule. It was synthesized following the method of Ogan *et al*. (32). This contrast agent has a distribution volume of 0.05 $l\ kg^{-1}$ and a plasma half-life of 3 h in rats. Albumin–$(Gd–DTPA)_{45}$ was injected at a dose of 0.03 $mMGd\ kg^{-1}$. The size of the MMCM molecule prevents leakage through properly matured vessels outside the tumor, resulting in a prolonged period of intravascular retention of the contrast agent. Only newly formed, hyper-permeable tumor vessels contribute to contrast extravasation. When evaluated with DCE-MRI, MMCM demonstrates *in vivo* imaging properties that correlate with histological features of angiogenesis (35).

4.3. Magnetic Resonance Imaging

MRI was performed using a clinical 1.5 T MRI scanner (Signa CVi, GE Healthcare, Milwaukee, WI, USA). A custom-made dedicated single-loop surface coil with an internal diameter of 1.7 cm was constructed specifically to create a high signal-to-noise ratio. The imaging protocol consisted of two consecutive sequences, a calibration and a dynamic scan. To estimate the $T_{1,0}$ of blood prior to contrast injection, a flow-compensated gradient echo inversion recovery echo planar imaging (IR GE-EPI) sequence (36) with 25 inversion time (*TI*) values (start: step: end = 100: 50: 1200 ms) was performed using a repetition time/echo time (*TR/TE*) of 15 000/24.3 ms, matrix of 128 × 128 with an in-plane resolution of 0.55 × 0.55 mm and slice thickness of 0.8 mm covering the entire tumor (30 slices, scan time 11 min). Dynamic images were acquired using a 3D T_1-weighted RF spoiled gradient echo sequence with imaging parameters *TR/TE* 12.37/2.95 ms, flip angle 18° and readout bandwidth 81 Hz per pixel. The matrix selected

was 256 × 256 × 64 with a field-of-view of 30 × 26 mm^2 leading to true voxel resolution of 0.12 × 0.14 × 0.50 mm^3. The temporal resolution was 3.1 min per 3D volume. The first 10 time points were acquired at a temporal resolution of 3.1 min. To sample the time frame efficiently, after the first 10 acquisitions, time gaps of 15 min were applied and after each gap two series were acquired. The total scan was acquired in approximately 90 min covering 16 time points.

4.4. Experimental Protocol

MRI was performed at baseline and 1 h after ILP (4). ILP intervention allows the delivery of high doses of cytostatic drugs by isolating the tumor-bearing limb from the systemic circulation. Briefly, the animals were anesthetized with ketamine and xylazine, and 50 units heparin were injected intravenously. The femoral artery and vein of anesthetized rats were cannulated with silastic tubing. Collaterals were occluded by groin tourniquet and perfusion was started after the tourniquet was tightened. An oxygenation reservoir and a roller pump were included in the circuit. The animals were randomly assigned to either the drug treatment or the control group and perfused with 5 ml Haemaccel (Behring Pharma, Amsterdam, The Netherlands) with hemoglobin of 0.9 mmol per l.50 g. In the drug treatment group, 50 μg TNF-α (Boehringer, Ingelheim, Germany) and 40 μg melphalan (Alkeran, Wellcome, Beckenham, UK) were added to the perfusate. In the control group no drugs were added to the perfusate. Perfusion was maintained for 30 min at a flow rate of 1.8 ml min^{-1}, and finalized by washout with 5 ml oxygenated Haemaccel. To restore physiological limb perfusion, the femoral artery was decannulated and sutured. During the ILP intervention and MRI imaging, the rat's temperature was maintained at 38–39 °C by means of a warm water mattress.

4.5. Motion Correction and Co-Registration

Spatial correspondence between MRI sequences is not always guaranteed; in particular, baseline and follow-up scans may not be aligned. In addition, the long MRI acquisition time complicates the co-registration problems. To perform a proper quantitative analysis the spatial relation between the sequences needs to be established. Therefore, we co-register the images before and after the intervention. Figure 7 shows the registration procedure. First, the intra-sequence motion correction was performed for both sequences separately. Second, the separate sequences were co-registered. Third, the late-stage enhanced image for follow-up was registered to the baseline image to ensure the spatial correspondence before and after treatment. All registration steps were performed using Elastix (37), first rigidly and then as an affine transformation.

4.6. Pharmacokinetic Modeling

The tumor contrast agent transport through the capillary plasma compartment was modeled by the Tofts model (38,39). The pharmacokinetic analysis of DCE-MRI requires estimates of the contrast concentration, $C(t)$. To estimate $C(t)$, a flow compensated

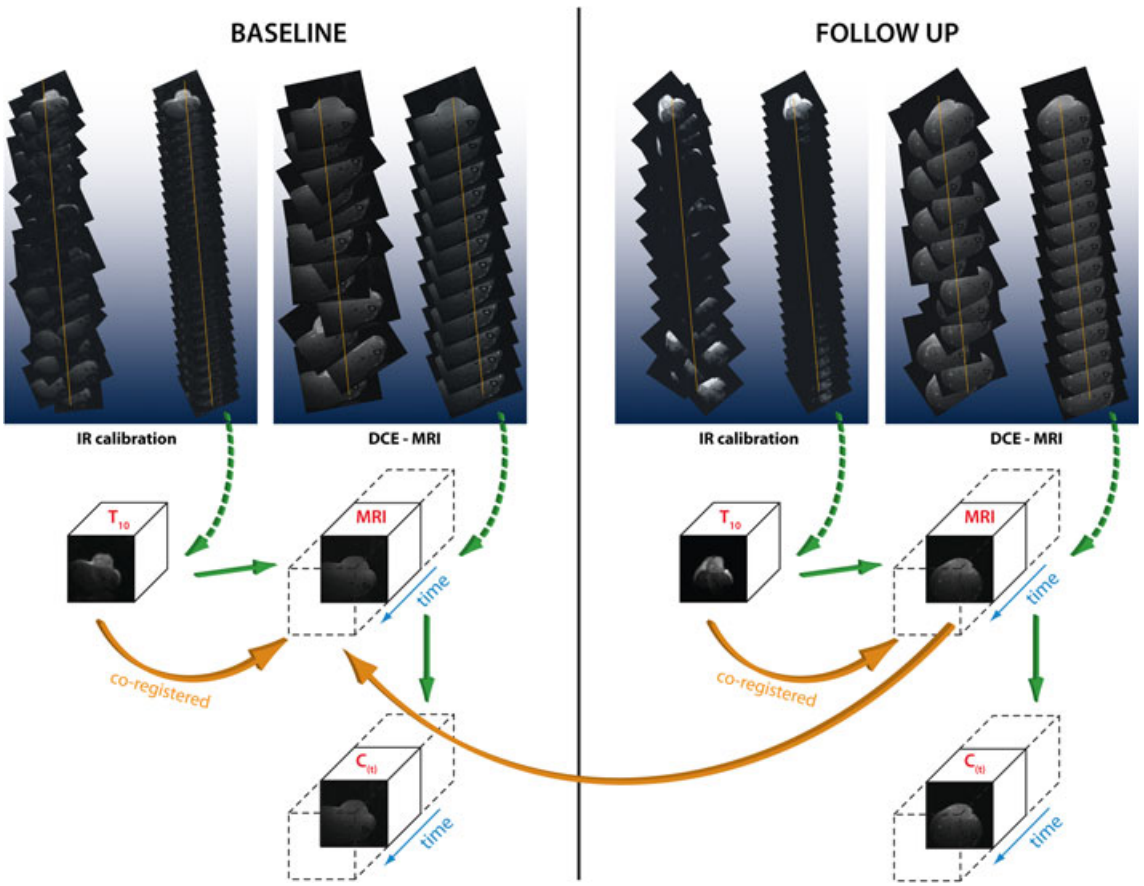

Figure 7. Overview of the registration steps at baseline (left-hand side) and follow-up (right-hand side) performed previous to pharmacokinetic analysis.

inversion recovery gradient echo planar imaging (IR-GE EPI) sequence was acquired prior to contrast injection. For each animal, longitudinal relaxation time ($T_{1,0}$) was estimated voxelwise by a nonlinear least-square fit of the acquired signal intensities $S(T_{In})$ against inversion times (40)

$$S(T_{In}) = c * \left(1 - 2e^{-\frac{T_{In}}{T_1}}\right) \quad (1)$$

To account for the incomplete clearance of the contrast agent after the intervention owing to the prolonged retention of MMCM in the intravascular space, pre-contrast $T_{1,0}$ is estimated at follow-up acquisitions as well.

The estimated $T_{1,0}$ was used in calculation of plasma contrast concentration over time, $C_p(t)$, and the tumor contrast concentration over time, $C_t(t)$. For both concentration curves, the molar concentration over time is defined by eqn (2) (41):

$$C(t) = \frac{1}{r_1} * [R_1(r) - R_1(0)] \quad (2)$$

where $R_{1,0}$ (= $1/T_{1,0}$) and $R_{1,t}$ represent the longitudinal relaxation rate of the tissue prior to and at different time points after the contrast agent injection; r_1 is the T_1 relaxivity of albumin–(Gd–DTPA)$_{45}$ at 1.5 T [0.273 M^{-1} s^{-1} (42)].

Expressing the enhancement of MRI signal intensity, for a GRE sequence (43), after the contrast agent injection and separating parameter A offers the molar concentration of the contrast agent over time [eqn (3)]:

$$A = \frac{S(t)}{S_0} * \frac{\left(1 - e^{-T_R/T_{10}}\right)}{\left(1 - \cos\alpha e^{-T_R/R_{10}}\right)}$$
$$C(t) = \frac{1}{r_1}\left[\frac{1}{T_R} * \ln\left[\frac{(1 - A\cos\alpha)}{(1 - A)}\right] - \frac{1}{T_{10}}\right] \quad (3)$$

For the plasma contrast concentration, often referred to as a VIF, we outlined manually a major tumor-feeding vessel in the latest contrast concentration image by using a VOI. By applying this VOI to all time points and spatial averaging, we created a contrast plasma concentration curve, $C_p(t)$. Subsequently, by assuming a bi-exponentially decaying VIF (44), we fitted $C_p(t)$ using the following function:

$$C_p(t) = a_1 e^{-m_1 t} + a_2 e1^{-m_2 t} \quad (4)$$

To compute K^{trans}, the estimated parameters a_1, a_2, m_1 and m_2 were used. The tumor contrast concentration curve $C_t(t)$ was fitted voxel-wise, by a nonlinear least-square fit, using eqn (5):

$$C_t(t) = DK^{trans}\sum_{n=1}^{2}\frac{a_i}{m_i - k_{ep}}\left(e^{-m_i t} - e^{-k_{ep}t}\right) \quad (5)$$

The fitting procedure resulted in a voxel-wise K^{trans} value and a coefficient of determination r^2. This coefficient summarizes the resemblance between observed values and the values expected under the Tofts model (38,39). The inherent image noise will mask low signal enhancement, resulting in low r^2. We excluded all voxels with $r^2 < 0.75$ from further analysis, since these voxels do not follow the Tofts model properly. Voxels with $r^2 > 0.75$ were identified as enhancing. The volume transfer constant, that is, K^{trans}, was presented as parametric maps before and after the intervention by ILP. DCE-MRI data analysis was performed using in-house developed software based on MATLAB (MathWorks, Natick, MA, USA). All steps were performed voxel-wise after motion correction and co-registration.

4.7. Tumor Features

The whole tumor was outlined manually by an experienced radiologist (C.F.v.D.) in the final DCE-MRI image. Using the whole tumor mask, we generated automatically the following masks (Fig. 8): tumor rim, tumor core, tumor periphery. The tumor rim was defined as the peripheral 10% of the tumor volume. The tumor core was defined as the 50% of the tumor diameter covering the tumor core. The tumor periphery was defined as the outer 50% of the tumor. Tumor core and periphery were automatically each subdivided into eight tumor sectors. Figure 8 shows the position of the various VOIs within a tumor. For whole tumor, tumor rim, tumor core, tumor periphery and for all 16 tumor sectors, we calculated first-order statistics (e.g. mean, median, standard deviation) of K^{trans}.

4.8. Cumulative Map-Volume Histogram

Cumulative dose-volume histograms have been used in radiotherapy to graphically summarize three-dimensional (3D) dose-distribution in two-dimensional graphs (45). This concept has been expanded to cumulative dose-[functioning]-mass histogram (D[F]MH) (46,47). To describe the 3D map distribution of a pharmacokinetic map, we propose a CMV histogram. Besides the origin of the information that it summarizes, the CMV histogram is identical to D[F]MH. The pharmacokinetic map is first divided into 50 equal bins (rather an arbitrary number). As we are primarily interested in the enhancing fraction, only the voxels belonging to this fraction were used for further analysis. The CMV histogram plots K^{trans} on the x-axis and percentage volume of the tumor (with $K^{trans} \geq$ that specific value) on the y-axis. The CMV always slopes from north-west to south-east and is usually a sigmoid shaped function. The slope of this function reflects the distribution of the K^{trans}, and was estimated (by a least squares fitting) for three categories of K^{trans} values ($0 < K^{trans} \leq 1$), ($1 < K^{trans} \leq 2$) and ($2 < K^{trans} \leq 5$). The distribution of all estimated slopes was captured per tumor as mean and standard deviation over all 16 sectors. The variance (or standard deviation) of slopes, between the regions, is a measure for tumor heterogeneity. To report the group trends for both distribution parameters, we computed the mean and

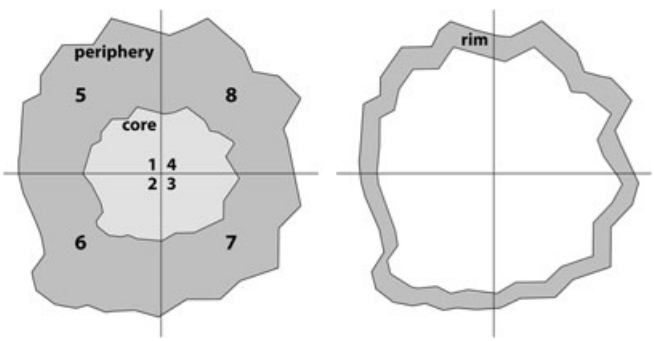

Figure 8. The tumour regions of interest (left-hand side) showing tumour periphery, tumour core and first eight tumour sectors. The tumour rim is shown on the right-hand side.

standard deviation over all animals belonging to a specific category (treated, sham, before treatment and after treatment). The slopes of the CMV histogram at baseline and follow-up are summarized in Table 2.

4.9. Statistical Analysis

Statistical analysis was performed using SPSS (SPSS for Windows, Version 17.0, SPSS Inc., Chicago, IL, USA). Two categories were defined: treated and sham. The Mann–Whitney *U*-test was used to assess differences between the two response categories based on the K^{trans} parametric map acquired before and after treatment. For the follow-up examination, the Wilcoxon signed rank test was used to assess the differences between the two response categories based on the K^{trans} parametric maps. A *p*-value of <0.05 was considered statistically significant.

Acknowledgments

Albumin–(Gd–DTPA)$_{45}$ was generously provided by Dr R. C. Brasch, Center of Pharmaceutical and Molecular Imaging, Department of Radiology, University of California San Francisco, CA, USA. This work was funded by NWO – Mozaiëk (grant no. 017.002.019) and an Erasmus MC seed grant. The funders had no role in study design, data collection and analysis, decision to publish or preparation of the manuscript.

REFERENCES

1. Jain RK, Duda DG, Willett CG, Sahani DV, Zhu AX, Loeffler JS, Batchelor TT, Sorensen AG. Biomarkers of response and resistance to antiangiogenic therapy. Nat Rev Clin Oncol 2009; 6(6): 327–338.
2. Duda DG, Ancukiewicz M, Jain RK. Biomarkers of antiangiogenic therapy: how do we move from candidate biomarkers to valid biomarkers? J Clin Oncol 2010; 28(2): 183–185.
3. Yang X, Knopp MV. Quantifying tumor vascular heterogeneity with dynamic contrast-enhanced magnetic resonance imaging: a review. J Biomed Biotechnol 2011; 2011: 732848.
4. Manusama ER, Stavast J, Durante NM, Marquet RL, Eggermont AM. Isolated limb perfusion with TNF alpha and melphalan in a rat osteosarcoma model: a new anti-tumour approach. Eur J Surg Oncol 1996; 22(2): 152–157.
5. Preda A, Wielopolski PA, Ten Hagen TL, van Vliet M, Veenland JF, Ambagtsheer G, van Tiel ST, Vogel MW, Eggermont AM, Krestin GP, van Dijke CF. Dynamic contrast-enhanced MRI using macromolecular contrast media for monitoring the response to isolated limb perfusion in experimental soft-tissue sarcomas. MAGMA 2004; 17(3–6): 296–302.
6. Seynhaeve AL, Eggermont AM, ten Hagen TL. TNF and manipulation of the tumor cell-stromal interface: 'ways to make chemotherapy effective'. Front Biosci 2008; 13: 3034–3045.
7. Hoving S, Brunstein F, aan de Wiel-Ambagtsheer G, van Tiel ST, de Boeck G, de Bruijn EA, Eggermont AM, ten Hagen TL. Synergistic antitumor response of interleukin 2 with melphalan in isolated limb perfusion in soft tissue sarcoma-bearing rats. Cancer Res 2005; 65(10): 4300–4308.
8. van der Veen AH, de Wilt JH, Eggermont AM, van Tiel ST, Seynhaeve AL, ten Hagen TL. TNF-alpha augments intratumoural concentrations of doxorubicin in TNF-alpha-based isolated limb perfusion in rat sarcoma models and enhances anti-tumour effects. Br J Cancer 2000; 82(4): 973–980.
9. de Wilt JH, Manusama ER, van Tiel ST, van Ijken MG, ten Hagen TL, Eggermont AM. Prerequisites for effective isolated limb perfusion using tumour necrosis factor alpha and melphalan in rats. Br J Cancer 1999; 80(1–2): 161–166.
10. Eggermont AM, Schraffordt Koops H, Klausner JM, Kroon BB, Schlag PM, Lienard D, van Geel AN, Hoekstra HJ, Meller I, Nieweg OE, Kettelhack C, Ben-Ari G, Pector JC, Lejeune FJ. Isolated limb perfusion with tumor necrosis factor and melphalan for limb salvage in 186 patients with locally advanced soft tissue extremity sarcomas. The cumulative multicenter European experience. Ann Surg 1996; 224(6): 756–764; discussion 764–755.
11. van Etten B, de Vries MR, van IMG, Lans TE, Guetens G, Ambagtsheer G, van Tiel ST, de Boeck G, de Bruijn EA, Eggermont AM, ten Hagen TL. Degree of tumour vascularity correlates with drug accumulation and tumour response upon TNF-alpha-based isolated hepatic perfusion. Br J Cancer 2003; 88(2): 314–319.
12. Padhani AR. Functional MRI for anticancer therapy assessment. Eur J Cancer 2002; 38(16): 2116–2127.
13. Zweifel M, Padhani AR. Perfusion MRI in the early clinical development of antivascular drugs: decorations or decision making tools? Eur J Nucl Med Mol Imag 2010; 37 suppl 1: S164–182.
14. Padhani AR. MRI for assessing antivascular cancer treatments. Br J Radiol 2003; 76(1): S60–80.
15. Daldrup-Link HE, Brasch RC. Macromolecular contrast agents for MR mammography: current status. Eur Radiol 2003; 13(2): 354–365.
16. Nelson DA, Tan TT, Rabson AB, Anderson D, Degenhardt K, White E. Hypoxia and defective apoptosis drive genomic instability and tumorigenesis. Genes Dev 2004; 18(17): 2095–2107.
17. Jain RK. Normalization of tumor vasculature: an emerging concept in antiangiogenic therapy. Science 2005; 307(5706): 58–62.
18. Seynhaeve AL, Hoving S, Schipper D, Vermeulen CE, de Wiel-Ambagtsheer G, van Tiel ST, Eggermont AM, Ten Hagen TL. Tumor necrosis factor alpha mediates homogeneous distribution of liposomes in murine melanoma that contributes to a better tumor response. Cancer Res 2007; 67(19): 9455–9462.
19. Alic L, Veenland JF, van Vliet M, van Dijke CF, Eggmont AMM, Niessen WJ. Quantification of heterogeneity in dynamic contrast enhancement MRI data for tumor treatment assessment. In IEEE International Symposium on Biomedical Imaging: From Nano to Macro, 6–9 April 2006, Arlington, VA.
20. Rose CJ, Mills SJ, O'Connor JP, Buonaccorsi GA, Roberts C, Watson Y, Cheung S, Zhao S, Whitcher B, Jackson A, Parker GJ. Quantifying spatial heterogeneity in dynamic contrast-enhanced MRI parameter maps. Magn Reson Med 2009; 62(2): 488–499.
21. Alic L, van Vliet M, van Dijke CF, Eggermont AM, Veenland JF, Niessen WJ. Heterogeneity in DCE-MRI parametric maps: a biomarker for treatment response? Phys Med Biol 2011; 56(6): 1601–1616.
22. Pickles MD, Manton DJ, Lowry M, Turnbull LW. Prognostic value of pre-treatment DCE-MRI parameters in predicting disease free and overall survival for breast cancer patients undergoing neoadjuvant chemotherapy. Eur J Radiol 2009; 71(3): 498–505.
23. Nagashima T, Sakakibara M, Nakamura R, Arai M, Kadowaki M, Kazama T, Nakatani Y, Koda K, Miyazaki M. Dynamic enhanced MRI predicts chemosensitivity in breast cancer patients. Eur J Radiol 2006; 60(2): 270–274.
24. van Rijswijk CS, Geirnaerdt MJ, Hogendoorn PC, Peterse JL, van Coevorden F, Taminiau AH, Tollenaar RA, Kroon BB, Bloem JL. Dynamic contrast-enhanced MR imaging in monitoring response to isolated limb perfusion in high-grade soft tissue sarcoma: initial results. Eur Radiol 2003; 13(8): 1849–1858.
25. Robinson SP, McIntyre DJ, Checkley D, Tessier JJ, Howe FA, Griffiths JR, Ashton SE, Ryan AJ, Blakey DC, Waterton JC. Tumour dose response to the antivascular agent ZD6126 assessed by magnetic resonance imaging. Br J Cancer 2003; 88(10): 1592–1597.
26. Gaustad JV, Benjaminsen IC, Ruud EB, Rofstad EK. Dynamic contrast-enhanced magnetic resonance imaging of human melanoma xenografts with necrotic regions. J Magn Reson Imag 2007; 26(1): 133–143.
27. Checkley D, Tessier JJ, Kendrew J, Waterton JC, Wedge SR. Use of dynamic contrast-enhanced MRI to evaluate acute treatment with ZD6474, a VEGF signalling inhibitor, in PC-3 prostate tumours. Br J Cancer 2003; 89(10): 1889–1895.
28. Benjaminsen IC, Graff BA, Brurberg KG, Rofstad EK. Assessment of tumor blood perfusion by high-resolution dynamic contrast-enhanced MRI: a preclinical study of human melanoma xenografts. Magn Reson Med 2004; 52(2): 269–276.
29. Benjaminsen IC, Brurberg KG, Ruud EB, Rofstad EK. Assessment of extravascular extracellular space fraction in human melanoma xenografts by DCE-MRI and kinetic modeling. Magn Reson Imag 2008; 26(2): 160–170.
30. Jia G, O'Dell C, Heverhagen JT, Yang X, Liang J, Jacko RV, Sammet S, Pellas T, Cole P, Knopp MV. Colorectal liver metastases: contrast agent diffusion coefficient for quantification of contrast enhancement heterogeneity at MR imaging. Radiology 2008; 248(3): 901–909.

31. Schwickert HC, Roberts TP, Shames DM, van Dijke CF, Disston A, Muhler A, Mann JS, Brasch RC. Quantification of liver blood volume: comparison of ultra short TI inversion recovery echo planar imaging (ULSTIR-EPI), with dynamic 3D-gradient recalled echo imaging. Magn Reson Med 1995; 34(6): 845–852.
32. ten Hagen TL, Eggermont AM, Lejeune FJ. TNF is here to stay – revisited. Trends Immunol 2001; 22(3): 127–129.
33. de Wilt JH, ten Hagen TL, de Boeck G, van Tiel ST, de Bruijn EA, Eggermont AM. Tumour necrosis factor alpha increases melphalan concentration in tumour tissue after isolated limb perfusion. Br J Cancer 2000; 82(5): 1000–1003.
34. Jackson A, Buckley D, Parker GJM. Dynamic Contrast-enhanced Magnetic Resonance Imaging in Oncology. Springer: Berlin, 2003.
35. Barrett T, Kobayashi H, Brechbiel M, Choyke PL. Macromolecular MRI contrast agents for imaging tumor angiogenesis. Eur J Radiol 2006; 60(3): 353–366.
36. Guo JY, Kim SE, Parker DL, Jeong EK, Zhang L, Roemer RB. Improved accuracy and consistency in T1 measurement of flowing blood by using inversion recovery GE-EPI. Med Phys 2005; 32(4): 1083–1093.
37. Klein S, Staring M, Murphy K, Viergever MA, Pluim JP. elastix: a toolbox for intensity-based medical image registration. IEEE Trans Med Imag 2010; 29(1): 196–205.
38. Tofts PS. Modeling tracer kinetics in dynamic Gd-DTPA MR imaging. J Magn Reson Imag 1997; 7(1): 91–101.
39. Tofts PS, Brix G, Buckley DL, Evelhoch JL, Henderson E, Knopp MV, Larsson HB, Lee TY, Mayr NA, Parker GJ, Port RE, Taylor J, Weisskoff RM. Estimating kinetic parameters from dynamic contrast-enhanced T(1)-weighted MRI of a diffusable tracer: standardized quantities and symbols. J Magn Reson Imag 1999; 10(3): 223–232.
40. Barral JK, Gudmundson E, Stikov N, Etezadi-Amoli M, Stoica P, Nishimura DG. A robust methodology for in vivo T1 mapping. Magn Reson Med 2010; 64(4): 1057–1067.
41. Bhujwalla ZM, Artemov D, Glockner J. Tumor angiogenesis, vascularization, and contrast-enhanced magnetic resonance imaging. Top Magn Reson Imag 1999; 10(2): 92–103.
42. Ogan MD, Schmiedl U, Moseley ME, Grodd W, Paajanen H, Brasch RC. Albumin labeled with Gd-DTPA. An intravascular contrast-enhancing agent for magnetic resonance blood pool imaging: preparation and characterization. Invest Radiol 1987; 22(8): 665–671.
43. Liney G. MRI from A to Z: a Definitive Guide for Medical Professionals. Springer; New York, 2010.
44. Weinmann HJ, Laniado M, Mutzel W. Pharmacokinetics of GdDTPA/dimeglumine after intravenous injection into healthy volunteers. Physiol Chem Phys Med NMR 1984; 16(2): 167–172.
45. Shipley WU, Tepper JE, Prout GR, Jr., Verhey LJ, Mendiondo OA, Goitein M, Koehler AM, Suit HD. Proton radiation as boost therapy for localized prostatic carcinoma. JAMA 1979; 241(18): 1912–1915.
46. Butler LE, Forster KM, Stevens CW, Bloch C, Liu HH, Tucker SL, Komaki R, Liao Z, Starkschall G. Dosimetric benefits of respiratory gating: a preliminary study. J Appl Clin Med Phys 2004; 5(1): 16–24.
47. Nioutsikou E, Webb S, Panakis N, Bortfeld T, Oelfke U. Reconsidering the definition of a dose-volume histogram. Phys Med Biol 2005; 50(11): L17–19.

